

Particle deconfinement in a bent magnetic mirror

Renaud Gueroult and Nathaniel J. Fisch

Princeton Plasma Physics Laboratory, Princeton University, Princeton, New Jersey 08543, USA

(Received 23 August 2012; accepted 18 October 2012; published online 6 November 2012)

Coils misalignment in a magnetic mirror can produce additional particle transport. The magnetic field non-axi-symmetry is responsible for radial and longitudinal drifts in a way much similar to the *neo*-classical transport in a tandem mirror cell distorted by end plugs. Accordingly, a regime exhibiting large radial displacements—similar to the resonant regime in tandem mirrors—can be obtained by confining ions azimuthally, for example by means of a properly tuned radial electric field. Because of the mass dependence of the magnetic field non-homogeneity drift velocities, the azimuthal trapping is mass specific, allowing, in principle, the filtering of a specific species based on its mass. © 2012 American Institute of Physics. [<http://dx.doi.org/10.1063/1.4765692>]

I. INTRODUCTION

The search for fusion plasma confinement devices has given rise to comprehensive studies of particle confinement in magnetic mirrors.^{1,2} The original concept relied on purely axi-symmetric magnetic fields,³ a configuration for which the first-order guiding center approximation theory predicts no particle drift across the magnetic fields surfaces. However, non-axi-symmetric magnetic fields were quickly introduced. Superposing a multi-pole type⁴ magnetic field to the magnetic mirror axi-symmetric field was suggested as a means to produce a magnetic well mirror field exhibiting plasma MHD stability.⁵ Later on, more complex configurations using *baseball* coil windings⁶ or *ying-yang* coils⁷ generalized the use of non-axi-symmetric magnetic fields in magnetic mirrors.

Following these developments, a number of peculiarities of particle confinement properties in non-axi-symmetric magnetic fields have been identified. In particular, it was shown that the *neoclassical transport*^{8,9} induced by the field non-axi-symmetry can, for specific resonance conditions, dominate over transport along the field lines through the mirror ends. The cancellation of successive radial drifts can be obtained in a tandem mirror by having one end plug rotated by $\pi/2$ with respect to the other one.¹⁰ Particular care is generally given to the magnetic coils alignment so as to minimize these effects in the central cell of a tandem mirror.¹¹ On the other hand, coils misalignment may be a desirable feature in specific configurations, such as the ELMO bumpy torus (EBT),¹² so the plasma properties in a canted mirror were also examined.^{13,14} The underlying idea was to ensure that the deviation from the parallel configuration is small enough for each single element of the EBT to be operated similarly to a parallel mirror. In other cases, one may be interested in enhancing these properties that are detrimental for confinement, for example, to filter a specific plasma population out of the device. Lately, there has been considerable interest, in fact, in plasma-based mass filters.^{15–18}

The introduction of a radial electric field produces azimuthal rotation which can in turn accomplish one of two things. If the azimuthal rotation is faster than the radial drift,

it can limit the radial displacement much as the rotational transform confines charged particles in a tokamak by limiting the vertical displacement. On the other hand, the imposed azimuthal rotation can also be used to cancel the natural azimuthal rotations so that ions are confined azimuthally and therefore deconfined radially.

In this paper, we show how to produce selective ion deconfinement in a bent magnetic mirror configuration. In Sec. II, the effects on the particle transport of the magnetic field non-axi-symmetry exhibited by a bent magnetic mirror configuration are identified. In Sec. III, the existence of a resonance-like effect when the particle is confined azimuthally is demonstrated, and the resulting radial motion is numerically evaluated. In Sec. IV, the mass dependence properties of the resonance-like effect are studied. The main findings are summarized in Sec. V.

II. NON AXI-SYMMETRY EFFECTS

The configuration considered is sketched in Fig. 1. It consists of a classic two-coil magnetic mirror, except that the coils are not properly aligned. Each coil is rotated by an angle α with respect to the axial plan of symmetry defined by $z = 0$. The magnetic field produced by this coil configuration can be described analytically by summing the individual contribution of each coil using elliptic integrals.¹⁹ Magnetic field maps obtained in different azimuthal planes and illustrating the tri-dimensional nature of the field are plotted in Fig. 2. This magnetic field solution is used to integrate ions trajectories solving the Lorentz equation by means of modified fourth order Runge-Kutta algorithm.²⁰ The time-step is typically taken equal to $1/20$ of the gyro-period at the particle current position which ensures energy conservation within 1% over the total integration duration.

Figure 3 presents the temporal evolution of the spatial coordinates (r, θ, z) of a Strontium ion initialized at $(r_0, \theta_0, z_0) = (0.2, 0, 0)$ with an initial kinetic energy $\varepsilon_0 = 15$ eV and a pitch angle equal to 15° . Three different time scales covering three orders of magnitude are observed. These three time scales correspond to the periodic motions associated with each of the three guiding center classical adiabatic invariants:²¹ the

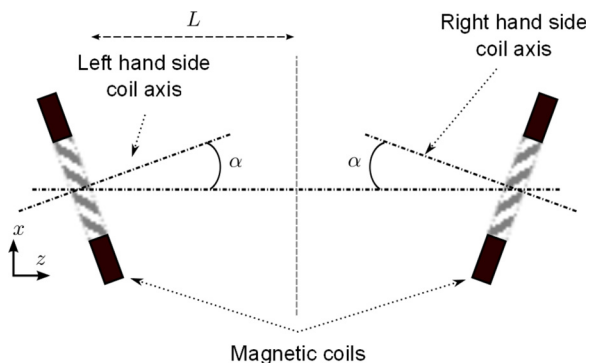


FIG. 1. Cut-view of the bent magnetic mirror configuration considered. Each coil is tilted by an angle α with respect to the longitudinal mid-plane. Coils are distant by $2L = 1$ m and are 15 cm in radius.

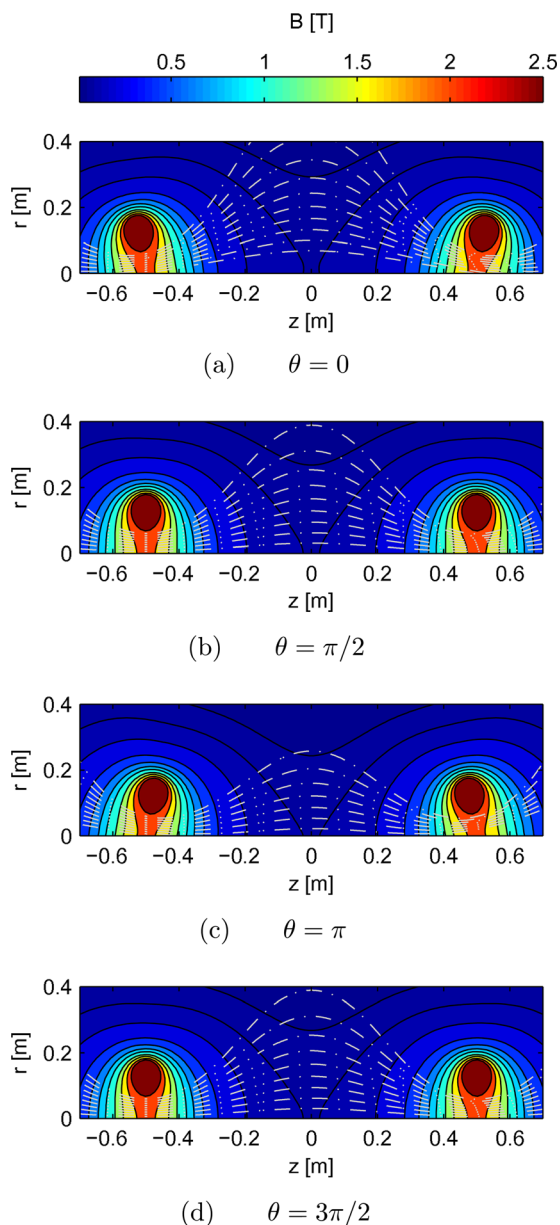


FIG. 2. Magnetic field intensity contours in four azimuthal planes ($\theta = \tan^{-1}(y/x)$). Gray dashed lines represent the projection of the magnetic field lines. Tilting angle $\alpha = 10^\circ$.

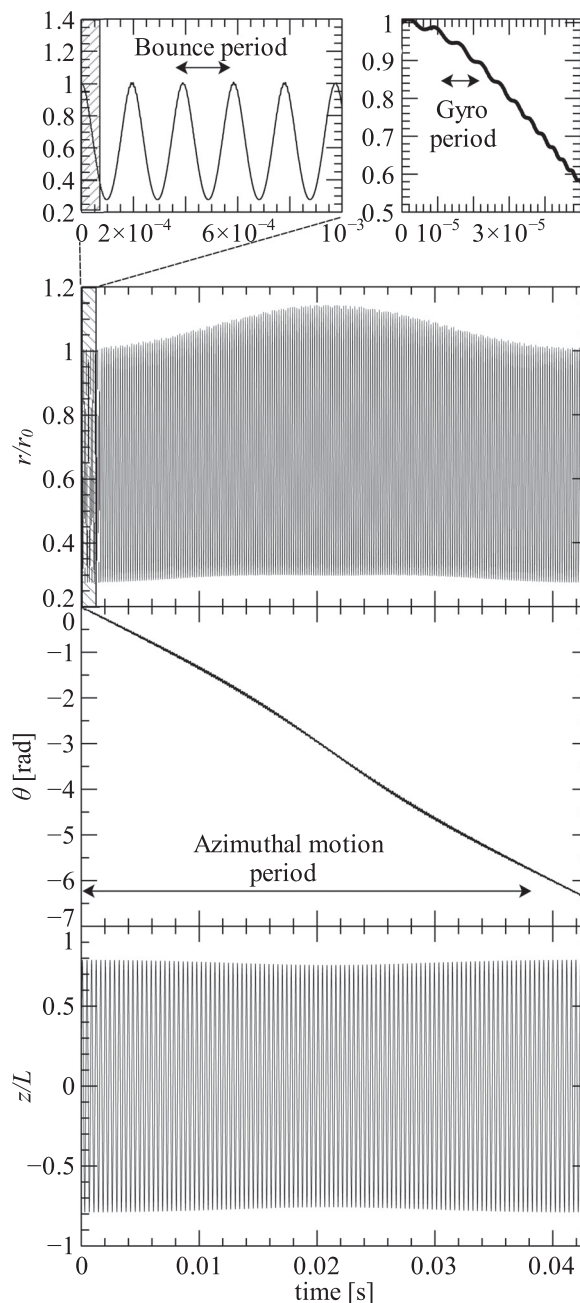


FIG. 3. Temporal evolution of the ion spatial coordinates. Multiple time scales are at play; the classic azimuthal motion periodicity observed in magnetic mirror is accompanied by radial and longitudinal displacement because of the magnetic field non axi-symmetry.

magnetic moment μ , the longitudinal adiabatic invariant, and the magnetic flux. The main difference as compared to a standard magnetic mirror configuration for which coils are parallel is the radial and longitudinal particle transport induced by the magnetic field non axi-symmetry. The characteristic time of this additional transport mechanism is the one of the azimuthal motion.

The ion motion perpendicular to the magnetic surface results from the combination of two effects: drifts perpendicular to the magnetic surface and a radial displacement arising from the non circularity of the magnetic surface.

More specifically, neglecting currents, the sum of the curvature and gradient drift reads as

$$\mathbf{V}_D = \frac{v_{\parallel}^2 \mathbf{R} \times \mathbf{b}}{\omega R^2} + \frac{v_{\perp}^2 \mathbf{b} \times \nabla B}{2\omega B} = \frac{v_{\parallel}^2 + v_{\perp}^2/2}{R^2\omega} \mathbf{R} \times \mathbf{b}, \quad (1)$$

where $B = |\mathbf{B}|$, $\mathbf{b} = \mathbf{B}/B$ is the unit vector along the magnetic field line, $\omega = qB/m$ is the ion gyro-frequency, R is the field line radius of curvature, and v_{\parallel} and v_{\perp} are, respectively, the parallel and perpendicular velocity components. Due to the tilting of the coils, b_{θ} and R_{θ} no longer vanish, which induces a drift in both the radial and longitudinal directions. Nevertheless, because of the configuration symmetry with respect to the xz plane, the drifts in each of the two half domains ($0 < \theta < \pi$ and $\pi < \theta < 2\pi$) tend to cancel.

In addition to these drifts perpendicular to the field lines, a displacement in the radial direction is observed as a result of the deformation of the magnetic surface, as depicted in Fig. 4. Because of the non circular profile of the magnetic surface in the longitudinal mid-plane, an ion moves away from the magnetic surface as it drifts azimuthally. The particle does not return to its initial radial position after a longitudinal bounce, with each bounce yielding a radial displacement with respect to the magnetic surface.

The radial displacements induced by these different effects are plotted in Fig. 5 along with the temporal evolution of the ion radial position in the longitudinal mid-plane as computed directly from the Lorentz equation. The sum of the displacements resulting from the different identified effects matches the direct integration of the Lorentz equation. The particle is alternatively inwardly and outwardly radially transported as the particle drifts azimuthally from one half domain $0 < \theta < \pi$ to the other one. Because of the configuration symmetry, the radial transport is on average balanced as the ion completes its azimuthal periodic drift motion. The amplitude of these radial oscillations is limited (about 20% of the initial radial coordinate r_0) but increases with the ion residence time in one half of the domain, that is to say, with a decrease of the pitch angle for a given particle energy.

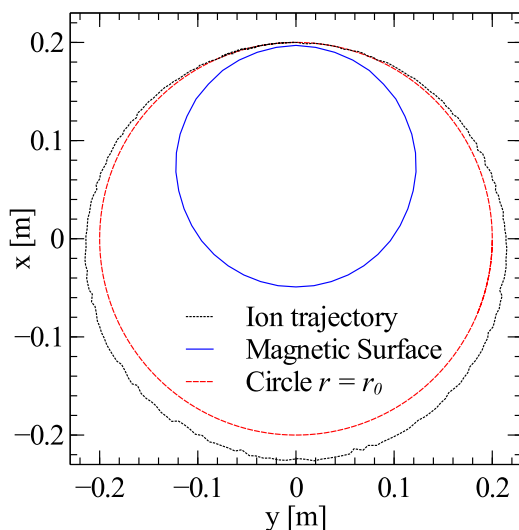


FIG. 4. Poincaré plot in the longitudinal mid-plane. The solid blue line is the magnetic surface passing by $(r_0, \theta_0) = (0.2, 0)$, the black dotted line is the ion orbit, and the red dashed line is the circle of radius r_0 .

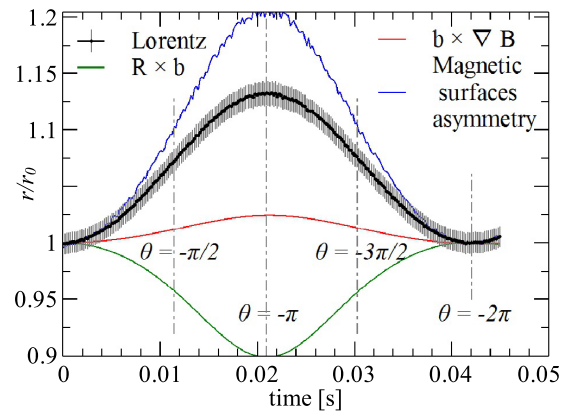


FIG. 5. Temporal evolution of the ion radial coordinate when crossing the $z = 0$ plane. Non axi-symmetry is responsible of the radial drift of the particle. Error bars correspond to the ion Larmor radius. The vertical dashed-dotted lines indicate the particle azimuthal position. The red and green curves are, respectively, the radial displacement induced by the gradient and the curvature drift. The solid blue curve is the radial displacement induced by the non circular profile of the magnetic surface in the longitudinal mid-plane.

The bent magnetic mirror radial transport depicted above is similar to that for a tandem mirror central cell distorted by end plugs in the regime where the azimuthal displacement per longitudinal bounce is limited.⁸ In the case of the bent mirror, the balancing of the radial displacements is obtained on a timescale of the order of the azimuthal motion period. On the other hand, radial transport balancing is achieved for each longitudinal bounce in a tandem mirror. Analogous to the resonance effect observed at higher rotation speed in tandem mirrors,⁸ the ion radial transport may be unbalanced in the bent mirror by confining the ion in half of the domain ($0 \leq \theta \leq \pi$ or $\pi \leq \theta \leq 2\pi$). Such an azimuthal confinement can be obtained, for example, by adding an inward radial electric field such that the $\mathbf{E} \times \mathbf{B}$ drift balances the azimuthal component of the curvature drift. Another way to produce the net radial ion drift would be to match the longitudinal ion displacements to the magnetic field curvature so that ion will have on average (on the ion path from the longitudinal mid-plane to the mirror reflection point) a zero azimuthal drift.

III. RESONANCE-LIKE PROPERTY

In this section, an external electric field is assumed to be constant and perpendicular to the magnetic surface everywhere: $\mathbf{E} = E_0 \mathbf{n}$, where \mathbf{n} is the radially inward normal vector to the magnetic surface. In other words, the magnetic flux surfaces are considered as equipotential surfaces. One way of obtaining an inwards pointing electric field consists in using multiple concentric charged electrodes in each magnetic coil plane.²² Although this technique may be inefficient for large plasma number densities, where the plasma natural positive charge resulting of the electron larger scattering rate might screen the externally applied electric field, it should be applicable for moderate plasma number densities. Another way of inducing rotation may lie in the use of waves.²³

Since the curvature and $\mathbf{E} \times \mathbf{B}$ drift velocities are position dependent, the balancing of their azimuthal components

cannot be achieved globally. It is nevertheless possible to tune E_0 so as to increase the ion residence time in azimuthal regions of interest. Figure 6 presents the temporal evolution of the particle radial position as it crosses the longitudinal mid-plane, along with the radial displacement produced by the different drifts, for a particle initialized close to an azimuthal equilibrium point. The $\mathbf{E} \times \mathbf{B}$ drift is not only responsible of the ion confinement in a limited azimuthal region but also contributes to the ion drift in the radial direction. Indeed, because of the non axi-symmetry of the magnetic field, since the electric field is assumed to be perpendicular to the magnetic surface everywhere, the $\mathbf{E} \times \mathbf{B}$ drift velocity has a radial component. The test ion is seen to reach a relatively large radial position in the device (measured in the longitudinal mid-plane). Quantitatively, the radial position increases by more than 60% in a third of the azimuthal motion period compared to without the electric field.

As the ion radial position increases, the $\mathbf{E} \times \mathbf{B}$ azimuthal drift velocity $V_\theta^{E \times B}$ decreases since the magnetic field intensity decreases. The curvature azimuthal drift velocity V_θ^{curv} decreases as the magnetic field line curvature increases with radius. Neglecting for a moment the mirror bending, the magnetic field intensity in the longitudinal mid-plane where the curvature is the larger decreases as $r^2/(L^2 + r^2)^{5/2}$, where L is the distance from one coil to the longitudinal mid-plane. In addition, an estimation of the field line curvature in the mid-plane can be obtained starting from the magnetic field components derived from the cylindrical expansion of the magnetic potential¹

$$B_r = B_0 \left[1 - \alpha \cos\left(\frac{\pi z}{L}\right) J_0\left(\frac{\pi r}{L}\right) \right], \quad (2a)$$

$$B_z = -B_0 \alpha \sin\left(\frac{\pi z}{L}\right) J_1\left(\frac{\pi r}{L}\right), \quad (2b)$$

with $\alpha < 1$ a constant related to the magnetic mirror ratio and J_0 and J_1 the Bessel functions of the first kind. Then, the field line curvature $\kappa = (\mathbf{b} \cdot \nabla)\mathbf{b}$ in the longitudinal mid-plane can be expressed as

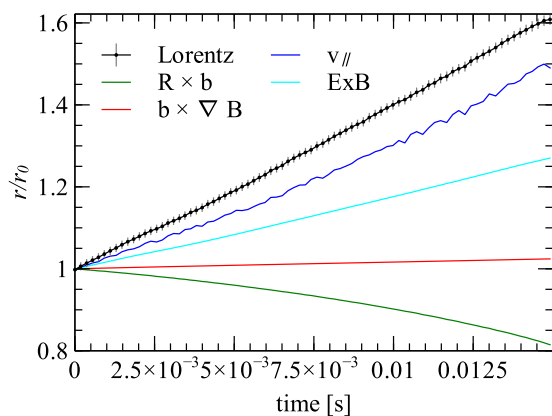


FIG. 6. Temporal evolution of the ion radial coordinate when crossing the $z=0$ plane. $\theta_0 = -\pi/2$. Azimuthal trapping in a given half of the domain allows the particle to reach large radial position in the mid-plane as compared to the passing orbits.

$$\kappa_r = -\frac{\pi \alpha J_1\left(\frac{\pi r}{L}\right)}{L \left[1 - \alpha J_0\left(\frac{\pi r}{L}\right) \right]} \underset{r \rightarrow 0}{\sim} -\frac{\pi^2 \alpha}{2(1-\alpha)L^2} r + O(r^3). \quad (3)$$

Accordingly, Eq. (1) indicates that the norm of the curvature drift azimuthal velocity in the mid-plane increases as $(L^2 + r^2)^{5/2}/r$. On the other hand, the $\mathbf{E} \times \mathbf{B}$ azimuthal drift velocity increases as $(L^2 + r^2)^{5/2}/r^2$. Putting together these results, we have $|\partial V_\theta^{E \times B} / \partial r| < |\partial V_\theta^{curv} / \partial r|$.

Consider now the azimuthal dependence of the drift velocities. Both the curvature and the $\mathbf{E} \times \mathbf{B}$ azimuthal drift velocity amplitudes decrease with θ for $0 \leq \theta \leq \pi$. Nevertheless, because of the decrease with θ of the magnetic field line radius of curvature R , $|\partial V_\theta^{E \times B} / \partial \theta| < |\partial V_\theta^{curv} / \partial \theta|$. Since the configuration is symmetric with respect to the $y=0$ plane, the result is, of course, the opposite one for $\pi \leq \theta \leq 2\pi$.

The ion orbits are depicted in Fig. 7. Assuming that the electric field is properly tuned so that different azimuthal drift velocities cancel at some given positions $(\tilde{r}, \tilde{\theta})$ in the mid-plane, an ion will either drift radially inward or outward depending on the sign of $\sin(\theta_0)$. In case the radial drift motion is inward ($0 \leq \theta_0 \leq \pi$) and for relatively large values of θ_0 , the $\mathbf{E} \times \mathbf{B}$ azimuthal drift velocity is larger than the curvature's one, and the particle starts a clockwise azimuthal motion until it reaches its symmetric position ($r=r_0, \theta=-\theta_0$). For smaller θ_0 values, the curvature drift velocity may be larger than the $\mathbf{E} \times \mathbf{B}$ drift velocity, in which case the particle first moves in a counter-clockwise direction. Nevertheless, as the radial coordinate decreases, the $\mathbf{E} \times \mathbf{B}$ drift velocity becomes larger than the curvature's one, and the azimuthal motion reverses. It then follows a symmetric trajectory until reaching the magnetic surface. Now, starting from the other half of the domain ($\pi \leq \theta_0 \leq 2\pi$), a similar situation occurs, but the radial motion is outward. The ion radial

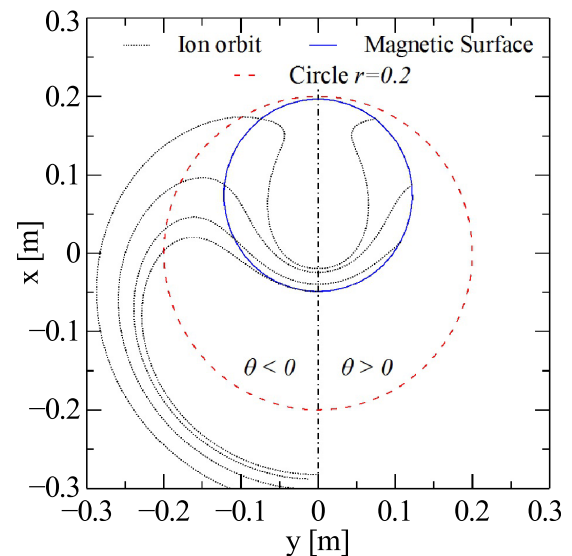


FIG. 7. Poincaré plot in the longitudinal mid-plane. The blue solid line is the magnetic surface passing by $(r, \theta) = (0.2, 0)$, the red dashed line is the circle $r=0.2$, the black dashed-dotted line delimits the two half domains, and the black dotted lines are the ion orbits for different initial positions on the magnetic surface. The $\mathbf{E} \times \mathbf{B}$ drift is counter-clockwise and the curvature drift is clockwise. $E_0 = 30 \text{ V m}^{-1}$, $\epsilon_0 = 15 \text{ eV}$.

position increases while moving in a clockwise manner until the curvature drift becomes larger than the $\mathbf{E} \times \mathbf{B}$ drift, where the azimuthal motion reverses. An increase of the ion radial coordinate up to 300% is observed as the particle is temporarily trapped in this region.

IV. MASS SELECTIVITY

Ions created, for example, by electron impact ionization would have zero kinetic energy in the lab frame. On the other hand, this ion will drift azimuthally at a speed equal to $(E_{z0}B_r - E_{r0}B_z)/B^2$ in the frame rotating at the $\mathbf{E} \times \mathbf{B}$ drift velocity. After pitch-angle scattering collisions, ions having different mass will conserve energy in the rotating frame but have different kinetic energies ε in the rest frame.

Because of the mass dependence of the field non-uniformity drifts as described by Eq. (1), ions of different masses will have different curvature and gradient drift velocities, but identical $\mathbf{E} \times \mathbf{B}$ drift velocities. Consequently, if an ion of a given mass is confined azimuthally by means of the $\mathbf{E} \times \mathbf{B}$ drift, another ion having a different mass will not. As the curvature drift velocity increases with the ion mass, the electric field value E_0 can be taken large enough so that the local balancing of azimuthal drift velocities will be achieved for heavy ions but not for light ions. In this case, light ions will have a positive azimuthal drift velocity everywhere and will exhibit clockwise azimuthal orbits. On the other hand, heavy ions will be trapped azimuthally.

This result is illustrated in Fig. 8, where the ion orbits obtained for the same electric field E_0 and same pitch angle as in Fig. 7 but a lower kinetic energy ε , i.e., representative of a lighter ion, are plotted. The light ion orbits are indeed passing, as opposed to the trapped orbits of heavier ions presented in Fig. 7, so that their radial displacement from the magnetic surface is limited. This mass selectivity could therefore be used to filter specific species by collecting the particles radially.

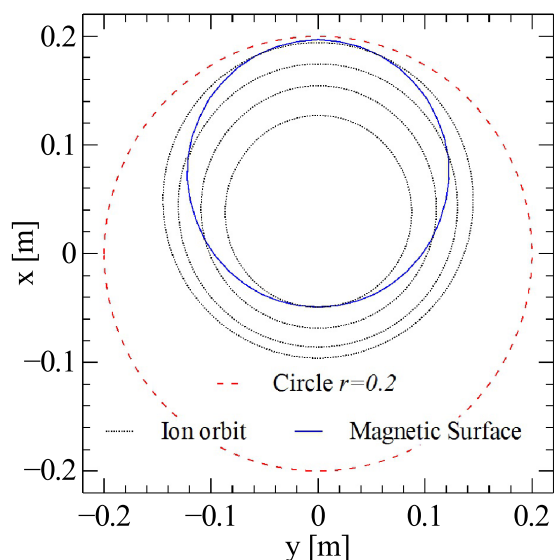


FIG. 8. Poincaré plot in the longitudinal mid-plane. The blue solid line is the magnetic surface passing by $(r_0, \theta_0) = (0.2, 0)$, the red dashed line is the circle $r=0.2$, and the black dotted lines are the ion orbits for different initial positions on the magnetic surface. $E_0 = 30 \text{ V m}^{-1}$, $e_0 = 5 \text{ eV}$.

Note that the azimuthal trapping makes more complex the filtering effect. Although the temporary azimuthal trapping is a mass dependent effect, it is also a pitch-angle dependent effect. Neglecting the gradient drift, if a particle \mathcal{B} of mass m_B is azimuthally trapped, then a particle \mathcal{A} of mass $m_A = \varrho^{-1}m_B$ will also satisfy the azimuthal trapping condition if $v_{A\parallel} = \sqrt{\varrho}v_{B\parallel}$. In separating \mathcal{B} from \mathcal{A} for $\varrho > 1$, the electric field E_0 would have to match the curvature drift of \mathcal{B} particles having small pitch angle so that it will be impossible for \mathcal{A} particles to have large enough v_{\parallel} to be trapped. Tuning the electric field so that the azimuthal confinement is achieved for high pitch-angles for the \mathcal{B} particle would produce radial extraction of a fraction of \mathcal{A} particles. This fraction increases significantly as the mass ratio ϱ gets closer to one, making it more difficult to distinguish by these means particles of nearly the same mass. In this regard, this separation mechanism is similar to the magnetic centrifugal mass filter,¹⁷ which also does not produce fine discrimination, but may have high throughput.

V. SUMMARY

Ion transport, induced by a coil misalignment in a bent magnetic mirror configuration, exhibits several unusual features. The non-alignment of magnetic coils in a magnetic mirror can yield *neo*-classical transport similar to that in non axi-symmetric tandem mirror cells. In the tandem mirror configuration, the radial displacements are balanced on average after each longitudinal bounce. In a bent mirror, the balancing is obtained only after a complete azimuthal period. Ions are shown to drift radially outward for half of an azimuthal motion period, while moving inward during the other half period.

In light of these results, a configuration using an inward external electric field was proposed so as to balance the azimuthal curvature drift by means of the $\mathbf{E} \times \mathbf{B}$ drift. When such an equilibrium is achieved, radial displacements can reach sufficiently large values for an ion to be collected radially before exiting the azimuthal region of interest. In order to take advantage of this behavior, one may capitalize on the equal velocity exhibited in the frame rotating at the $\mathbf{E} \times \mathbf{B}$ drift velocity by ions of different masses created with zero velocity in the lab frame. Since the curvature drift velocity is proportional to the ion mass, the electric field can be tuned to enhance radial displacement of specific species based on their mass.

Although this technique could, in principle, discriminate elements based on their mass, it remains to address the practical parameter space for such a mass separation device. In particular, the collisionality is expected to play a significant role. On the one hand, ion-ion collisions are desirable to the extent that redirecting the ion velocity along the field lines increases the drift velocity (Eq. (1)). On the other hand, the thermalization of two ion species of different mass towards a common ion temperature would mitigate the mass selectivity of the device since the drift velocity is proportional to the ion energy. More complex electric field structure might optimize the concept, notably by allowing a true azimuthal confinement rather than a temporary trapping.

ACKNOWLEDGMENTS

This work was supported by US DOE under Contract Nos. DE-FG02-06ER54851 and DE-AC02-09CH11466.

- ¹R. F. Post, *Nucl. Fusion* **27**, 1579 (1987).
²D. Ryutov, *Nucl. Fusion* **20**, 1068 (1980).
³G. I. Budker, *Plasma Physics and The Problem of Controlled Thermonuclear Reactions* (Pergamon, New York, 1959), Vol. 3, pp. 1–34.
⁴Y. V. Gott, M. S. Ioffe, and V. G. Telkovsky, *Nucl. Fusion Suppl.* **3**, 1045 (1962).
⁵J. Berkowitz, K. O. Friedrichs, H. Goertzel, H. Grad, J. Killeen, and E. Rubin, in *Proceedings of 2nd U.N. International Conference on Peaceful Uses of Atomic Energy*, United Nations, Geneva, 1958, Vol. 31, p. 171.
⁶C. C. Damn, J. H. Foote, A. H. Futch, R. K. Goodman, F. J. Gordon, A. L. Hunt, R. G. Mallon, K. G. Moses, J. E. Osher, R. F. Post, and J. F. Steinhilber, in *Proceedings of the 2nd Conference on Plasma Physics and Controlled Nuclear Fusion Research*, Novosibirsk, 1968, Vol. 2, p. 253.
⁷R. Moir and R. F. Post, *Nucl. Fusion* **9**, 243 (1969).
⁸D. D. Ryutov and V. Stupakov, *JETP Lett.* **26**, 174 (1977).
⁹D. D. Ryutov and V. Stupakov, *Sov. J. Plasma Phys.* **4**, 278 (1978).
¹⁰L. Lao, R. Conn, and J. Kesner, *Nucl. Fusion* **18**, 1308 (1978).
¹¹R. S. Post, J. W. Coleman, J. H. Irby, M. M. Olmstead, and R. P. Torti, *Rev. Sci. Instrum.* **56**, 1139 (1985).
¹²R. A. Dandl, “The ELMO bumpy torus experiment,” Technical Report No. ORNL TM-3694 (ORNL, 1971).
¹³R. Dandl, H. Eason, A. England, and J. Sprott, *Nucl. Fusion* **13**, 693 (1973).
¹⁴S. Hiroe, J. C. Glowienka, D. L. Hillis, J. B. Wilgen, G. L. Chen, J. A. Cobble, A. M. El Nadi, J. R. Goyer, L. Solensten, W. H. Casson, O. E. Hankins, and B. H. Quon, *Phys. Fluids* **30**, 847 (1987).
¹⁵T. Ohkawa and R. L. Miller, *Phys. Plasmas* **9**, 5116 (2002).
¹⁶R. Freeman, S. Agnew, F. Anderegg, B. Cluggish, J. Gilleland, R. Isler, A. Litvak, R. Miller, R. O’Neill, T. Ohkawa, S. Pronko, S. Putvinski, L. Sevier, A. Sibley, K. Umstadter, T. Wade, and D. Winslow, *AIP Conf. Proc.* **694**, 403 (2003).
¹⁷A. J. Fetterman and N. J. Fisch, *Phys. Plasmas* **18**, 094503 (2011).
¹⁸R. Gueroult and N. J. Fisch, “Practical considerations in realizing a magnetic centrifugal mass filter,” *Phys. Plasmas* (submitted).
¹⁹J. C. Simpson, J. E. Lane, C. D. Immer, and R. C. Youngquist, “Simple analytic expressions for the magnetic field of a circular current loop,” Technical Report No. 20010038494 (NASA, 2001).
²⁰J. Berland, C. Bogey, and C. Bailly, *Comput. Fluids* **35**, 1459 (2006).
²¹T. G. Northrop, *The Adiabatic Motion of Charged Particles*, *Interscience Tracts on Physics and Astronomy* (Interscience, New York, 1963).
²²G. Abdrashitov, A. Beloborodov, V. Volosov, V. Kubarev, Y. Popov, and Y. Yudin, *Nucl. Fusion* **31**, 1275 (1991).
²³A. J. Fetterman and N. J. Fisch, *Phys. Rev. Lett.* **101**, 205003 (2008).